Solid-State Fluorescence from Carbon Dots through Surface-Ligand Modification for Latent Fingerprint Visualization

M.Sc. Thesis

By

Khushi Jain

DEPARTMENT OF CHEMISTRY

INDIAN INSTITUTE OF TECHNOLOGY INDORE

May 2025

Solid-State Fluorescence from Carbon Dots through Surface-Ligand Modification for Latent Fingerprint Visualization

A THESIS

Submitted in partial fulfilment of the
requirements for the award of the degree
of
Master of Science

By

KHUSHI JAIN

DEPARTMENT OF CHEMISTRY

INDIAN INSTITUTE OF TECHNOLOGY

INDORE

May 2025

INDIAN INSTITUTE OF TECHNOLOGY INDORE

CANDIDATE'S DECLARATION

I hereby certify that the work which is being presented in the thesis entitled **Solid-State Fluorescence from Carbon Dots through Surface-Ligand Modification for Latent Fingerprint Visualization** in the partial fulfillment of the requirements for the award of the degree of **MASTER OF SCIENCE** and submitted in the **DEPARTMENT OF CHEMISTRY, Indian Institute of Technology Indore**, is an authentic record of my work carried out during the time period from July 2024 to May 2025 under the supervision of Prof. Shaikh M. Mobin, Associate Professor.

The matter presented in this thesis has not been submitted by me for the award of any other degree of this or any other institute.

Khushi Jain
19/5/25

Signature of the student with date
(NAME OF THE M.Sc. STUDENT)

This is to certify that the above statement made by the candidate is correct to the best of my/our knowledge.

M. Shaikh
May 20, 2025

Signature of Supervisor with date
(Prof. SHAIKH M. MOBIN)

KHUSHI JAIN has successfully given her M.Sc. Oral Examination held on **14.05.2025**.

ACKNOWLEDGEMENTS

This work could not have been executed without a great deal of guidance and support. I would like to sincerely thank those who provided me with everything I needed during my project. I wish to express my feelings to those whose support and motivation made it possible to present my research work.

First and foremost, I would like to thank my thesis supervisor, Prof. Shaikh M. Mobin, for his valuable guidance, suggestions, supervision, and continuous encouragement throughout my research work. I am highly obliged to take the opportunity to sincerely thank all the faculty members and SIC staff of IIT INDORE for their help and cooperation during this work. I would also like to thank IIT Jammu, JNCASR, Bangalore, IIT Gandhinagar, and HSGVV, Sagar, for their characterization facilities.

A heartfelt thanks to Ms. Nirmiti Mate for her unwavering support and advice. I am also thankful to Safwana Shirin and Afrin Asmat, and all the research scholars, my lab mates, who have contributed to an enriching and collaborative research environment. Also, I would like to thank Shaurya Aneja and Mridul Shyam Singhal for their constant support throughout my work. I want to extend my thanks to my batchmates who were always there. Finally, my deepest gratitude goes to my family, whose love, patience, and constant belief in me have been my greatest strength. This thesis would not have been possible without the support of every one of you.

KHUSHI JAIN

Dedicated to…

My Family

ABSTRACT

Latent fingerprints (LFPs) imaging is the most important approach to identify individuals, and there is a persisting need for the development of simple, rapid, accurate, and universal LFPs recognition methods. As the Carbon dots (CDs), being quasi-spherical in shape, exhibit unique physical, chemical, and optical properties, making them propitious for multifaceted usage. The nitrogen-doped CDs were synthesised from potassium humate as a carbon precursor and oPD as a nitrogen dopant via a one-step hydrothermal method. The obtained CDs have a particle size in the range of 2-9 nm with a quantum yield (QY) of 8.9%. However, obtaining CDs with multicolor emission in the solid state remains a great challenge, as typical aggregation-induced fluorescence quenching occurs in powder forms. Moreover, the construction of CDs with color-tunable solid-state fluorescence (SSF) has limited reports. Herein, through a surface ligand modification strategy, SSF CDs were prepared. Their emission wavelengths range from the yellow to the pink region were obtained. The multicolor SSF CDs are potentially utilized in the field of latent fingerprint visualization. The LFPs are detected with high resolution through the powder method on various substrates such as glass slide, cover slip, amber color glass bottle, aluminium foil, and steel. Also, their second and third-level substructures are clearly identified. The method is validated for LFPs visualization on different substrates and can also be stable up to around 30 days. The results demonstrate that the SSF CDs as a developer have great potential in LFP imaging for forensic investigation.

TABLE OF CONTENTS

LIST OF FIGURES	1-2
LIST OF SCHEMES	3
LIST OF TABLES	4
LIST OF ABBREVIATIONS	5
LIST OF ACRONYMS	6
CHAPTER 1: INTRODUCTION	7-8
CHAPTER 2: OBJECTIVES	9
CHAPTER 3: MOTIVATION	10
CHAPTER 4: LITERATURE REVIEW	11-12
CHAPTER 5: EXPERIMENTAL SECTION	13
5.1 Materials and Reagents	13
5.2 Instrumentation	13-14
5.3 Synthesis of N-hCDs	14
5.4 Synthesis of SSF powders	14-15
5.5 Quantum yield measurement	15
5.6 Latent Fingerprint Development	15
CHAPTER 6: RESULTS AND DISCUSSION	16
6.1 Morphological and Surface Characterisation of N-hCDs	16-17
6.2 Photophysical analysis of N-hCDs	17
6.3 Study of fluorescence stability	18
6.4 Quantum yield measurement	18
6.5 Characterization of SSF powders	19-23
6.6 Application for Latent fingerprint visualization and identification	23-26
CHAPTER 7: CONCLUSIONS AND SCOPE OF WORK	27
REFERENCES	28-31

LIST OF FIGURES

Figure 1. (a) Schematic of ACQ (left) and AIE (right) effects in CDs, (b) Examples of AIE luminogens.

Figure 2. (a) TEM image, (b) the corresponding histogram showing the size distribution, (c) HR-TEM image showing (100) lattices, (d) FT-IR spectrum, (e) XRD pattern, (f) XPS survey scan. A high-resolution XPS spectrum of (g) C1s, (h) N1s, and (i) O1s XPS spectra of N-hCDs.

Figure 3. Optical Characterization of N-hCDs (a) UV-vis spectra (inset: images of solution under visible and UV light), (b) FL emission spectra, (c) TCSPC measurements. The stability plots at different (d) pH, (e) temperatures.

Figure 4. Integrated fluorescence intensity against absorbance plots for: (a) quinine sulphate (QS) at 345 nm, (b) N-hCD at 280 nm. R^2 is the linear regression coefficient.

Figure 5. (a) Absorption spectra of (i) I@N-hCDs and (ii) B@N-hCDs, (b) PL emission spectra of (i) I@N-hCDs and (ii) B@N-hCDs.

Figure 6. (a) XPS survey spectra of both SSF powders (i) I@N-hCDs and (ii) B@N-hCDs. Deconvoluted spectra of I@N-hCDs and B@N-hCDs (b and c) C1s, (d and e) N 1s, (f and g) O 1s.

Figure 7. (a) FT-IR spectra of (i) I@N-hCDs and (ii) B@N-hCDs, (b) PXRD pattern of (i) I@N-hCDs, (ii) I-cB, (iii) B@N-hCDs, and (iv) dhB.

Figure 8. Photo images of I@N-hCDs and B@N-hCDs in H_2O (left) and EtOH (right) under visible and 365 nm irradiation. SEM images of (c) I@N-hCDs and (d) B@N-hCDs after being dispersed in water, confocal fluorescence images of (e) I@N-hCDs and (f) B@N-hCDs, (g) TGA curves of (i) I@N-hCDs and (ii) I@N-hCDs.

Figure 9. Developed fingerprint images of B@N-hCDs on (a) glass slide, (b) aluminum foil, (c) stainless steel bottle, (d) cover slip, and (e)

glass bottle of chemical under UV irradiation (upper) and visible light (lower).

Figure 10. Developed fingerprint images of I@N-hCDs on (a) glass slide, (b) aluminum foil, (c) stainless steel bottle, (d) cover slip, and (e) glass bottle of chemical under UV irradiation (upper) and visible light (lower).

Figure 11. (ai, ii) Images of LFPs on the aluminum foil developed through powder method with B@N-hCDs under UV light. The magnified images show specific details as listed below: (1) core, (2) hook, (3) bifurcation, (4) island, (5) termination, (6) sweat pores, and (7) scar.

Figure 12. Images of LFPs on the glass slide developed through powder method with I@N-hCDs under UV light. The magnified images show specific details as listed below: (1) core, (2) crossover, (3) termination, and (4) scar.

LIST OF SCHEMES

Scheme 1. Schematic for the synthesis of N-hCDs.

Scheme 2. Schematic for the synthesis of I@N-hCDs and B@N-hCDs.

LIST OF TABLES

Table 1. Represents the properties such as QY and emission behaviours of various materials in a solid state.

Table 2. The peak positions and the corresponding functional groups present in the deconvoluted XPS spectra of (a) I@N-hCDs and (b) B@N-hCDs.

Table 3. List of CD-based composites with SSF used for LFP visualization on various surfaces.

ABBREVIATIONS

ºC	Degree Celsius
a.u.	Arbitrary unit
mg	Milligram
h	Hour
mL	Milliliter
min	Minute
mmol	Millimole
eV	Electron Volt
min	Minutes
mV	Millivolt
nm	Nanometer
º	Degree
Conc.	Concentration
rpm	Revolutions per minute
wt.	weight
HOMO	Highest occupied molecular orbital
LUMO	Lowest unoccupied molecular orbital
η	Refractive index
Φ	Quantum yield

ACRONYMS

CDs	Carbon dots
ACQ	Aggregation-caused quenching
AIE	Aggregation-induced emission
SSF	Solid state fluorescence
oPD	o-phenylenediamine
LFP	Latent fingerprint
QD	Quantum dots
FP	Fingerprint
QS	Quinine sulphate
QY	Quantum Yield
dhB	2,4-dihydroxybenzaldehyde
I-cB	Indole-3-carboxaldehyde
FL	Fluorescence
UV-Vis	Ultraviolet-visible
PL	Photoluminescence
XPS	X-ray photoelectron spectroscopy
TGA	Thermogravimetric analysis
PXRD	Powder X-Ray Diffraction
ATR-FTIR	Attenuated total reflectance- Fourier transform infrared
TCSPC	Time-correlated single-photon counting
SEM	Scanning Electron Microscopy
TEM	Transmission Electron Microscopy
N-hCDs	Nitrogen-doped potassium humate derived CDs
B@N-hCDs	dhB-derived SSF-CDs
I@N-hCDs	I-cB-derived SSF-CDs

Chapter 1

INTRODUCTION

The distinctiveness and immutability of fingerprints make them a crucial aspect for identifying an individual worldwide. The judiciary considers fingerprints as the most reliable evidence in investigating crime scenes. FPs are formed due to the transfer of natural oils, sweat, lipids, and other residues from the skin when a finger comes in contact with a surface.[1] However, the FPs are mostly invisible at the crime scenes. So, to visualize these latent fingerprints (LFPs), various methods have been employed, including powder dusting, mass spectroscopy, fuming, chemical staining, photo-acoustic visualization, etc. Nonetheless, their applicability for rapid onsite development of LFPs is limited as nearly all of these techniques demand costly and non-portable equipment and show poor contrast.[2] The powder method for fingerprint development that depends on the powder's ability to adhere to the residues of FP has always been the most reliable technique during forensic investigation.[3] This method illustrates low background interference, high sensitivity, good contrast, and they are practical for on-the-spot utilization.[4]

Recently, rare-earth nanocrystals,[5] fluorescent polymer nanoparticles,[6] dye powders, perovskite nanostructures,[7] ferric oxide,[8] Mn^{4+}-doped red-emissive phosphors,[9] and AIE luminogens[10] have been frequently reported as potent fingerprint developers. Nevertheless, the costliness, potential toxicity, challenging preparation routes, and low stability of these materials limit their usage in the real world.[1] In recent times, carbon dots (CDs) have garnered significant attention for their use as LFP developers because of their high biocompatibility, facile and low-cost synthesis, prominent photoluminescence, non-toxicity, abundance of precursor molecules, etc.[1] However, while obtaining CDs in solid-state, they pose a drawback. The fluorescence of CDs gets quenched by the non-radiative loss of the excitons by energy transfer within the conjugated π-domains formed by π–π stacking of carbon cores.[3] This phenomenon is called Aggregation-caused Quenching (ACQ). To

overcome ACQ in solid-state, various methodologies have been explored to inhibit the π–π stacking and acquire Aggregation-induced emission (AIE). The CDs are incorporated with starch, polymers, inorganic solid matrix, and metal-organic framework (MOF) to get solid-state fluorescence (SSF) in CDs. Also, to prevent the π–π stacking, several AIEgens are used to modify the CDs' surface so that the AIE-active CDs are produced with enhanced SSF.[11] The mechanism of ACQ and AIE and some examples of AIEgens are shown in Figure 1.

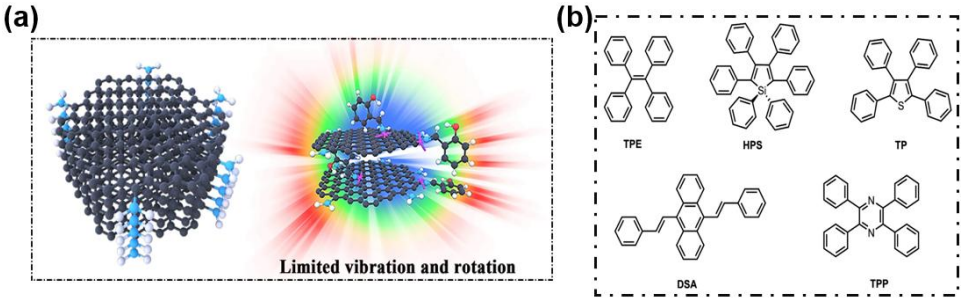

Figure 1. (a) Schematic of ACQ (left) and AIE (right) effects in CDs,[5] (b) Examples of AIE luminogens.[12]

In this work, we have prepared N-hCDs with bright orange FL, using potassium humate as a carbon precursor and o-phenylenediamine (oPD) to enhance the FL via N-doping. The N-hCDs are extensively characterized using various characterization techniques. Furthermore, the synthesized CDs are modified with 2,4-dihydroxybenzaldehyde (dhB) and Indole-3-carboxaldehyde (I-cB), separately through simple stirring via condensation to get the SSF powders B@N-hCDs and I@N-hCDs, emitting yellow and pink FL under UV radiation, respectively. The SSF powders are analysed by exploiting different morphological, structural, and optical characterization techniques. To prevent ACQ, a functionalization strategy has been implemented to procure SSF powders, which resulted in the formation of hydrogen bonds among the ligands and the carbon core, promoting radiative decay of excitons in an aggregate state. The obtained powders exhibit SSF under UV irradiation. The synthesized powders can be applied in the field of forensic science for LFP detection.

Chapter 2

OBJECTIVES

The main aim of this project is to functionalize the CDs with different ligands, thereby achieving the solid-state FL powders. CDs have been explored in various fields such as biomedical, optoelectronics, catalysis, forensics, etc., but the π-π stacking interactions in CDs result in the nonradiative loss of the excited state, causing the quenching of fluorescence in the solid-state, and this phenomenon is called as ACQ, which confines the versatility of CDs. Because of their special optical characteristics, which include excellent stability and powerful photoluminescence, solid-state CDs have gained attention as a potential material for fingerprint development. The use of solid-state carbon dots in fingerprint development offers a modern, efficient, and safer alternative to conventional methods as they are non-toxic, versatile, easy to apply, and durable.

- To synthesize N-doped CDs using potassium humate as a carbon source and o-phenylenediamine (oPD) as a dopant.
- To prevent ACQ, modified CDs are synthesized using different ligands to obtain aggregation-induced emission
- The 2,4-dihydroxybenzaldehyde (dhB) and Indole-3-carboxaldehyde (I-cB) ligands are reacted with N-hCDs to procure N-hCDs with color-tunable SSF.
- The obtained SSF powders are further utilized for latent fingerprint development in forensic science.

Chapter 3

MOTIVATION

Lately, high-tech biometrics have become popular as a result of the growing need for improved personal data protection. Data collection, identity verification in airports, and safer financial transactions are now possible owing to the integration of biometrics with Internet technologies. Computer security, forensics, and mobile applications all benefit from biometrics. Also, in the investigation of criminal cases, fingerprint detection plays a significant role in establishing whether a suspect is guilty or not. For the past several decades, fingerprints have been collected on plastic fingerprint cards or paper using ink, a slab, or a roller. Although fingerprints from clean hands are invisible to the naked eye, they can be disclosed by applying luminescent powders.[13–16] Iodine fuming, ninhydrin spraying, and powder dusting are some of the techniques that are used to improve the optical contrast of LFPs.[17]

These techniques, however, are not appropriate for on-site investigations in many complex instances involving fingerprint detection because of their poor adhesion, limited sensitivity, incapacity to identify fingerprints over extended periods, high cost, and environmentally harmful consequences.[18] Fluorescent nanoparticles, such as quantum dots (QDs), have been proposed as fluorescent probes because of their optical properties, which can improve optical contrast, sensitivity, and selectivity.[19] CDs are a viable alternative as they are non-toxic, biocompatible, and stable.

Chapter 4

LITERATURE REVIEW

In the past few decades, various fingerprint development methods have been explored by exploiting the fluorescence (FL) properties of various nanomaterials. FL imaging is a popular approach for LFP in conventional methods, including ferric oxide staining,[8] ninhydrin spraying,[20] iodine/cyanoacrylate fuming,[21] aluminium dusting,[22] etc.[23] Various spraying methods have also been explored with carbon dots for the development of FP. CDs serve as an efficacious fluorescent sensor due to their excellent biocompatibility and remarkable luminescence properties. CDs are quite versatile and exploited in a wide array of applications, including photodynamic treatment, photocatalysis, drug delivery, energy storage, bioimaging, sensing, and more.[24] The abundance of diverse precursor molecules and easy synthesis pathways allows for tailored functional groups on carbon dots (CDs), enhancing their surface reactivity.

However, these traditional methods have some restrictions, such as challenging preparation routes, destructive detection processes, high-cost synthesis, potential toxicity, and instability in practical environments.[25] Various compounds (like zinc carbonate, ferric oxide, titanium oxide, etc.) are utilized as spraying agents for the development of LFPs but there are certain drawbacks to this method such as background interference, upliftment of FPs, poor contrast due to ridges of FP, and also environmental factors like contamination with other substances, humidity, etc.[26,27] Conventionally, CDs in solution state were also used for FP detection. However, whereas standard CDs exhibit brilliant fluorescence in solution, solution-casting is inconvenient for permeable surfaces, including cardboard, wood, paper, and fabric.[25,28]

In recent years, the focus of scientists has shifted towards the synthesis of solid-state CDs. Moreover, when solutions of CDs are dried to get

CDs in a solid state, their FL gets quenched due to aggregation.[25] The π-π stacking in CDs results in the nonradiative loss of the excited state electrons, causing the quenching of fluorescence in the solid state, and this phenomenon is called aggregation-caused quenching (ACQ), which greatly limits the use of CDs in white light-emitting diodes (WLEDs) and the formation of CD-based high-efficiency irradiation and display devices.[5,19] To prevent the graphitized cores from aggregating, further techniques are also used, like dispersion of CDs into a polymer matrix such as starch, inorganic salts, silicon-based coupling compounds, polymer, and MOF.[31,32] Many strategies have been investigated to get around this aggregation-caused solid-state FL quenching; for example, Park et al. constructed graphene quantum dots arranged in a curved bowl shape, and Yang et al. successfully prevented π-π stacking by adding functional peripheral ligands to the CD surface.[33,34]

Chapter 5

EXPERIMENTAL SECTION

5.1 Materials and Reagents

2,4-dihydroxybenzaldehyde (dhB) and Indole-3-carboxaldehyde (I-cB) were purchased from Sigma Aldrich. Potassium humate, o-phenylenediamine, and NaOH were procured from SRL chemicals, Lobachem, and Rankem, respectively, and 98% H_2SO_4 was bought from Emplura. All the chemicals were used without any further treatment, and the experiments were performed using Milli-Q water. All the chemicals utilized are of analytical grade. The feather brush used for fingerprint application was procured from RIVEA REMEDIES LLP.

5.2 Instrumentation

5.2.1 UV-Visible Spectrophotometer

The UV-visible (UV-vis) absorption spectra were recorded on a Shimadzu UV-1900 spectrophotometer using a quartz cell (1 cm × 1 cm) and corrected against the solvent as the baseline.

5.2.2 Fluorescence Spectrophotometer

Fluorescence spectra were taken in a quartz cell (1 cm × 1 cm) on a fluoromax-4-spectrofluorometer.

5.2.3 X-Ray Diffractometer

An Empyrean X-ray Diffractometer from PANalytical with Cu Kα radiation was used to perform XRD to get insights about the crystallinity of carbon dots.

5.2.4 ATR-Fourier-Transform Infrared Spectrometer

This technique is used to determine the surface functionalities of carbon dots. The BRUKER ALPHA II instrument was used to obtain the IR spectra.

5.2.5 Time-correlated single-photon counting

The PL lifetime decays were measured from the TCSPC spectrometer of HORIBA Jobin Yvon of the Fluorocube-01-NL model. All the decay was then analysed with IBH DAS 6.0 software, and the sample was excited through a 280 nm picosecond diode laser.

5.2.6 Transmission Electron Microscope

TEM was used to determine the morphology of carbon dots. The TEM images were obtained using a FEI Tecnai G2 F30 S-Twin transmission electron microscope.

5.2.7 Field-Emission Scanning Electron Microscope

The samples were coated with gold to make them conductive, and images were taken using Zeiss Gemini-SEM 360.

5.2.8 X-ray photoelectron spectroscopy

The presence of surficial groups and the elemental composition of carbon dots were analysed through this technique.

5.2.9 Confocal Microscopy

The confocal microscopic technique was used to determine the distribution of CDs, and the confocal images were recorded on FV1200 MPE.

5.2.10 Thermogravimetric analysis (TGA)

The thermal stability of CDs was monitored using TGA on METTLER TOLEDO TGA/DSC 1 STARe System.

5.3 Synthesis of N-hCDs

The N-hCDs were synthesized from 100 mg of the potassium humate, which was weighed and added to the beaker containing 20 ml of Milli-Q water. The above reaction mixture was sonicated for 30 min, followed by the addition of 50 mg of oPD in the same reaction mixture, and further sonicated for 30 min. After that, 10 wt.% H_2SO_4 is added to this solution and transferred mixture in a Teflon-lined autoclave, and treated

hydrothermally at 180 ºC for 12 h. Further, the as-obtained N-hCDs were centrifuged at around 5000 rpm for 10 minutes and utilized.

5.4 Synthesis of SSF powders

5.4.1 CDs Modified with 2,4-dihydroxybenzaldehyde

The SSF powder B@N-hCDs was synthesized from dhB. For that purpose, 450 mg of dhB and 5 mL of N-hCDs were added to a 25 mL round-bottomed flask and refluxed at 85 ºC for 2 h via condensation reaction. Once the reaction mixture had cooled to room temperature, it was dialyzed for 18 h. Finally, the mixture was freeze-dried to produce CDs with yellow color solid-state fluorescence.

5.4.2 CDs Modified with Indole-3-carboxaldehyde

The SSF powder I@N-hCDs was synthesized from I-cB. For that purpose, 450 mg of I-cB and 5 mL of N-hCDs were added to a 25 mL round-bottomed flask and refluxed at 85 ºC for 2 h via condensation reaction. Once the reaction mixture had cooled to room temperature, it was dialyzed for 18 h. Finally, the mixture was freeze-dried to procure CDs with pink color solid-state fluorescence.

5.5 Quantum Yield Measurement

The quantum yield (Φ_S) of N-hCDs was calculated by Eq. 1. The N-hCDs FL QY was measured using quinine sulphate ($\Phi = 0.54$) dissolved in 0.1 M H_2SO_4 as a standard.

$$\Phi_S = \Phi_{QS} \times \frac{S_S}{S_{QS}} \times \frac{A_{QS}}{A_S} \times \frac{\eta_S^2}{\eta_{QS}^2} \quad (1)$$

Here, Φ_S and Φ_{QS} represent the quantum yields of the sample and the standard, respectively. S_S and S_{QS} are the integrated intensities of the sample and the standard, respectively, obtained from the plot of the FL integrated intensity versus the absorbance shown in Figure 3. A_S and A_{QS} denote the absorbance of the standard and the sample at λex 280 nm and 345 nm, respectively. η_S and η_{QS} are the refractive indices of the solvents used for the sample and standard, respectively.

5.6 Latent Fingerprint Development

The fingerprints were collected from the right thumb of a female donor. Firstly, she washed her hands thoroughly and dried them. Then, she rubbed the right thumb on the forehead and nose to evenly spread the eccrine sweat and sebaceous sweat across the ridges of the thumb. Then, the thumb was touched on various substrates, including a glass slide, aluminium foil, a cover slip, a glass bottle, and a steel bottle to widen the applicability of our SSF powders. The SSF powder was spread around the LFP, and the excess of it was brushed off using a feather brush. The developed FP was then irradiated with UV light (365 nm). Finally, the images were captured using an iPhone 11.

Chapter 6

RESULTS AND DISCUSSION

6.1 Morphological and Surface Characterisation of N-hCDs

The N-hCDs were synthesized using a simple single-step hydrothermal method utilizing potassium humate and oPD as a carbon precursor and nitrogen dopant, respectively, as shown in Scheme 1. The doping of CDs with nitrogen can widely enhance their fluorescent property, improving contrast and leading to better stability.[35]

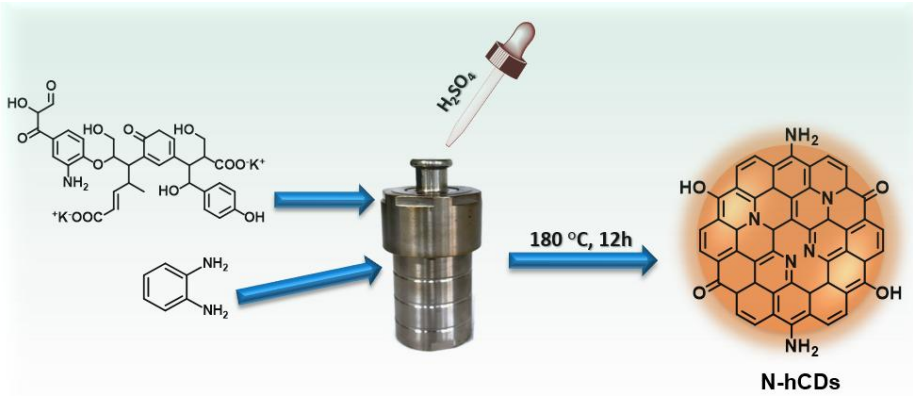

Scheme 1. Schematic for the synthesis of N-hCDs.

As shown in Figure 2a, the low-resolution TEM images of N-hCDs indicate that the CDs are well dispersed throughout the matrix. The size distribution of CDs is between 2-9 nm, shown in Figure 2b, with the mean diameter of 5.7 nm. The high-resolution TEM (HR-TEM) shown in Figure 2c depicts the d-spacing of 0.22 nm, which corresponds to the (100) graphitic plane. The functional moieties present on the surface of CDs are further characterized through the ATR-FTIR spectrum. As represented in Figure 2d, the FTIR spectra of N-hCDs, the intense peaks at 3713 cm^{-1}, 1750 cm^{-1}, 1189 cm^{-1}, 1080 cm^{-1}, and 591 cm^{-1} are assigned to OH/NH stretching, C=O stretching, C-O-C stretching, C-N/C-O stretching, and C-S bending, respectively. The XRD pattern of the N-hCDs (Figure 2e) exhibits a broad peak at around $2\theta = 23.48°$ associated with the (002) graphite plane. To get better insights into the chemical composition of N-hCDs, XPS

analysis was performed. Figure 1f represents XPS survey spectra of N-hCDs, which shows three peaks at 285, 402, and 533 eV, confirming the presence of C, N, and O. Figure 2g depicts the high-resolution XPS spectra of C1s, containing peaks at 285, 286.4, and 287.2 eV originating from sp^2 C (C–C / C=C), sp^3 C (C–O / C–N), and C=O / C=N, respectively. The N1s deconvoluted spectra (Figure 2h) show two peaks at 399.44 and 401.5 eV, indicating the presence of pyridinic and graphitic N, respectively. However, the O1s band was split into two peaks at 531.9 and 532.66 eV, which are assigned to C=O and C–O, respectively, shown in Figure 2i.

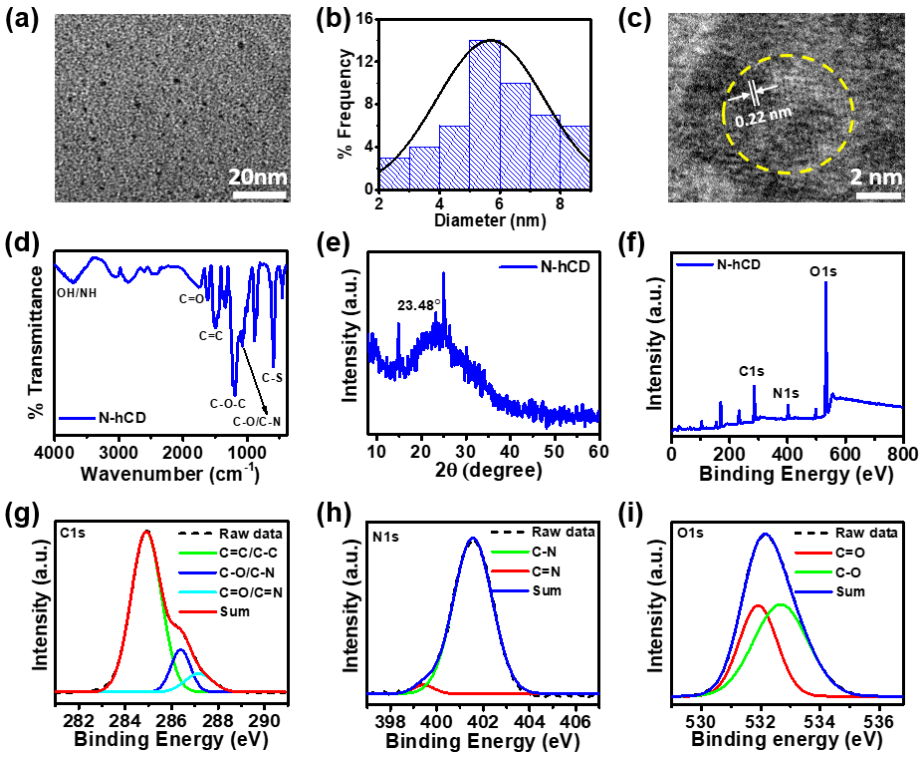

Figure 2. (a) TEM image, (b) the corresponding histogram showing the size distribution, (c) HR-TEM image showing (100) lattices, (d) FT-IR spectrum, (e) XRD pattern, (f) XPS survey scan. A high-resolution XPS spectrum of (g) C1s, (h) N1s, and (i) O1s XPS spectra of N-hCDs.

6.2 Photophysical analysis of N-hCDs

The optical properties of N-hCDs were determined using UV-vis and FL spectroscopy. The UV-vis spectrum shows peaks at 277 nm, which arises due to π- π* transition, along with a peak at 407 nm, which is assigned

to n- π* transition as depicted in Figure 3a. The N-hCDs possess a bright orange FL under UV irradiation (Figure 3a; inset). The FL spectrum of N-hCDs given in Figure 3b shows excitation-dependent emission behavior with altering intensities with excitation wavelength ranging from 280 to 370 nm. The maximum emission was observed at 339 nm against an excitation wavelength of 280 nm. The excitation-dependent behavior of N-hCDs is generally attributed to the distribution of varied sizes of CDs and the presence of discrete surface states.[26,15] Further, the fluorescence lifetime of N-hCDs was calculated using the TCSPC technique and evaluated as 1.31 ns by using a diode laser of 280 nm (Figure 3c). The curve was best fitted with a three-exponential function.

6.3 Study of fluorescence stability

Stability of CDs is a critical aspect, and it was determined under various conditions of temperature and pH. Figure 3d represents the stability plot of N-hCDs at different pH, and it was observed that the FL emission was fairly stable in the pH range 1-11. Furthermore, the FL intensities of N-hCDs were measured at different temperatures varying from -65 °C to 100 °C, and it was concluded that the FL emission was stable, retaining 90% FL (Figure 3e).

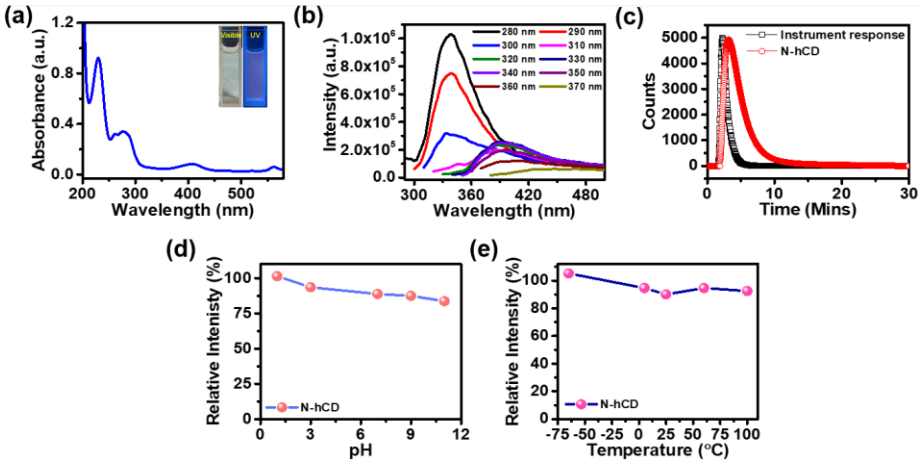

Figure 3. Optical Characterization of N-hCDs (a) UV-vis spectra (inset: images of solution under visible and UV light), (b) FL emission spectra, (c) TCSPC measurements. The stability plots at different (d) pH, (e) temperatures.

6.4 Quantum Yield Measurement

The quantum yield (Φ) of N-hCDs was calculated to be 8.89% at an excitation wavelength of 280 nm, having QS (Φ = 0.54) as a reference standard with a bright blue FL.

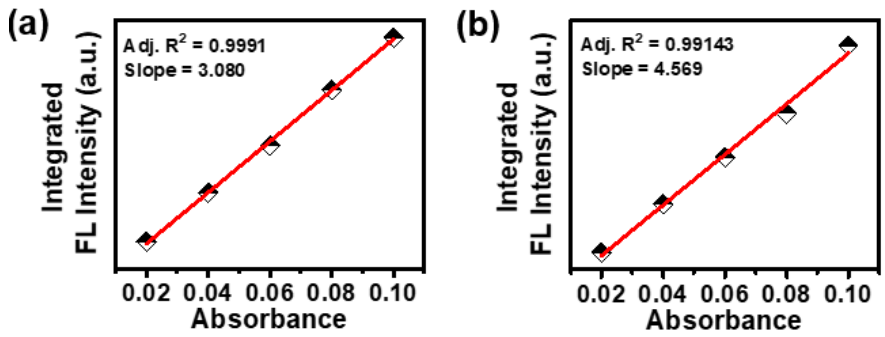

Figure 4. Integrated fluorescence intensity against absorbance plots for: (a) quinine sulphate (QS) at 345 nm, (b) N-hCD at 280 nm. R^2 is the linear regression coefficient.

6.5 Characterization of SSF powders

Further, the N-hCDs were modified with different ligands to obtain the FL in the solid state. The surface functionalization of CDs with different ligands plays a vital role in synthesizing CDs with aggregation-induced emission (AIE). The N-hCDs were functionalized with dhB and I-cB, synthesized through a condensation reaction, which gives yellow and pink SSF powders B@N-hCDs and I@N-hCDs as depicted in the digital photograph of Scheme 2. Table 1 indicates the comparative literature for various solid-state CDs and their properties, such as QY and emission behaviours.

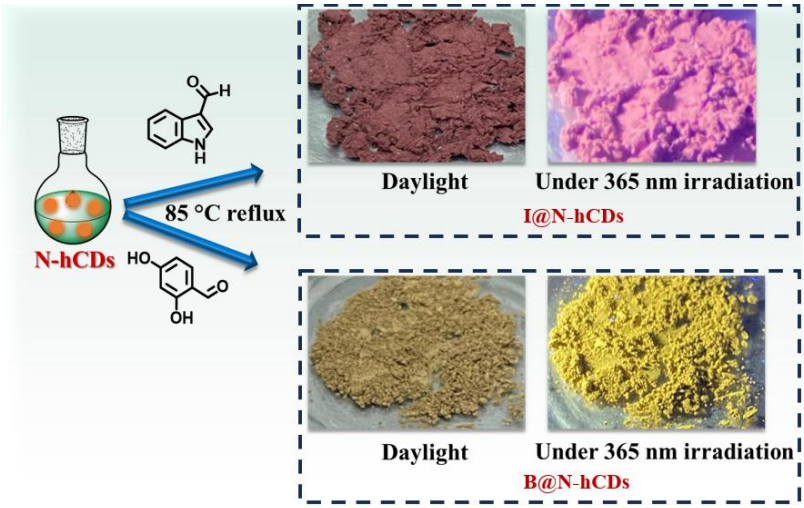

Scheme 2. Schematic for the synthesis of I@N-hCDs and B@N-hCDs.

S. No	CDs based composites	QY (%)	λ_{em} (nm)	References
1.	CD1	65	550	*ACS Appl. Mater. Interfaces* **2019**, *11*, 24395–24403
2.	H-CDs	5.96	620	*Nat Commun* **2019**, *10*, 1789-1800
3.	hr-CDs	1.22	550	*ACS Omega* **2020**, *5*, 11842–11848
4.	ScCDs	51.7	447	*Dalton Trans.*, **2021**, *50*, 12188-12196
5.	CD1:0.1	9	465	*ACS Appl. Nano Mater.* **2021**, *4*, 6386–6397
6.	O-CDs@PS films	1.69	511	*Chem. Commun.*, **2023**, *59*, 4475-4478
7.	diISA-CDs	1.76	726	*Angew. Chem. Int. Ed.* **2023**, *62*, e202217822
8.	R-CDs	10.5	630	*Inorg. Chem.* **2024**, *63*, 19827–19834
9.	B@N-hCDs	3.52	520	Our work
10.	I@N-hCDs	4.22	625	Our work

Table 1. Represents the properties such as QY and emission behaviours of various materials in a solid state.

The photophysical properties of B@N-hCDs and I@N-hCDs were investigated using UV-vis spectroscopy. The absorption spectra show a broad absorption range from 200 – 800 nm, indicated in Figure 5ai and ii, which arises due to π- π* and n- π* transitions. Figure 5bi and ii represent PL emission spectra for B@N-hCDs and I@N-hCDs. However, in the case of I@N-hCDs, the PL spectrum majorly shows two emission states, with maximum emission at 625 nm. But, in B@N-hCDs, the maximum emission is at 520 nm; however, in the instance of I@N-hCDs, the PL spectrum majorly shows two emission states,

with maximum emission at 625 nm. The origin of the multiple emissive states in PL spectra can be attributed to the surface defects on the CDs.[38] Functional groups containing heteroatoms like N and O, dangling bonds, sp^3 and sp^2 hybridized carbon atoms, and radiation less transitions are some of the factors that can create localized energy levels inside the band gap of CDs. Here, the excitons can be trapped and cause emissions related to surface defects.[39,40]

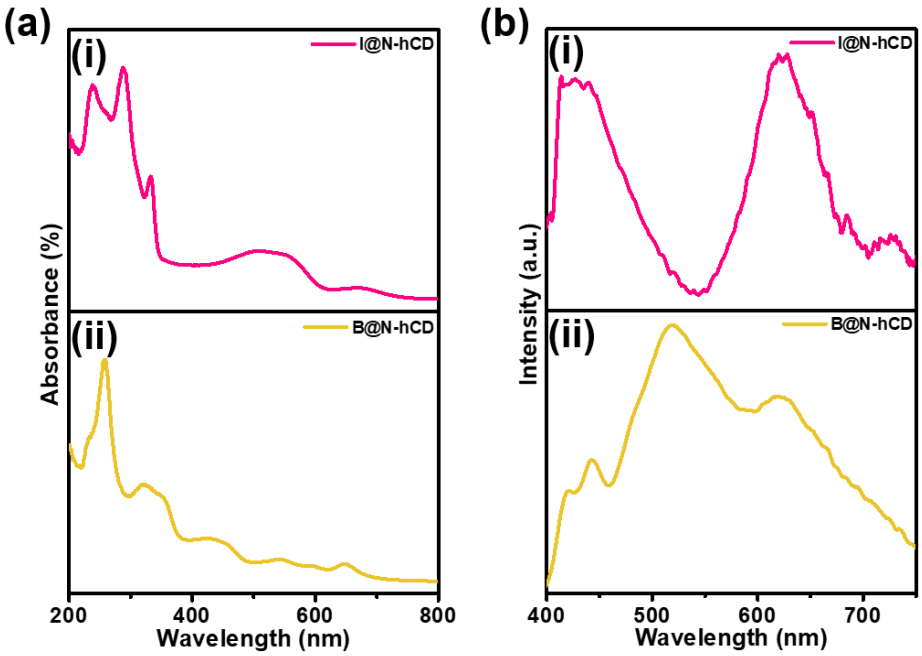

Figure 5. (a) Absorption spectra of (i) I@N-hCDs and (ii) B@N-hCDs, (b) PL emission spectra of (i) I@N-hCDs and (ii) B@N-hCDs.

To investigate the chemical composition of SSF powders, XPS study was carried out. XPS spectra of I@N-hCDs and B@N-hCDs are shown in Figure 6ai and ii, which reveal three peaks, which are attributed to C1s (284.08 eV), N1s (400.08 eV), and O1s (532.08 eV). Figures 6b-g show the high-resolution spectra of C1s, N1s, and O1s for both the SSF powders, and the results for deconvolution are indicated in Table 3.

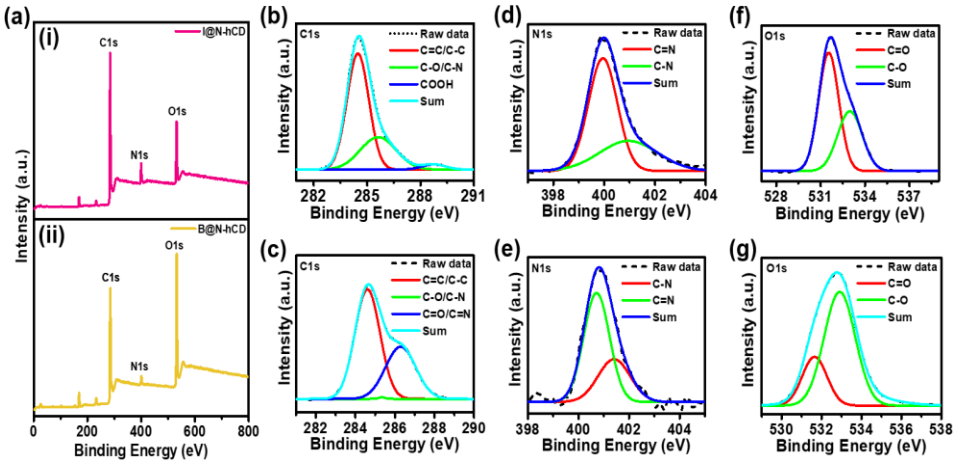

Figure 6. (a) XPS survey spectra of both SSF powders (i) I@N-hCDs and (ii) B@N-hCDs. Deconvoluted spectra of I@N-hCDs and B@N-hCDs (b and c) C1s, (d and e) N 1s, (f and g) O 1s.

(a)

I@N-hCDs		
Elements	**Chemical State**	**Binding Energy (eV)**
C1s	C = C / C – C	284.48
	C – O / C – N	285.62
	COOH	288.76
N1s	C – N	400.96
	C = N	399.95
O1s	C = O	531.54
	C – O	532.98

(b)

B@N-hCDs		
Elements	**Chemical State**	**Binding Energy (eV)**
C1s	C = C / C – C	284.61
	C – O / C – N	285.34
	C = O / C = N	286.28
N1s	C = N	400.71
	C – N	401.41
O1s	C = O	531.64
	C – O	532.91

Table 2. The peak positions and the corresponding functional groups present in the deconvoluted XPS spectra of (a) I@N-hCDs and (b) B@N-hCDs.

After functionalization of N-hCDs with I-cB and dhB, the FTIR spectra of I@N-hCDs indicate that the bands obtained at 3164 cm^{-1}, 1634 cm^{-1}, and 750 cm^{-1} arise due to OH/NH, C=N, and Ar-H, respectively (Figure 7ai), and for B@N-hCDs the bands arose at 3118 cm^{-1} (OH), 1615 cm^{-1}

(C=N), and 740 cm^{-1} (Ar-H) (Figure 7aii). The shifting and formation of new bands confirm that the ligands were successfully attached to the carbon core. The PXRD pattern of I@N-hCD and B@N-hCD shows some additional sharp peaks than those demonstrated by dhB and I-cB ligands, as shown in Figure 7bi-iv, which are associated with the crystalline domain created by ligands on the surface of CDs.

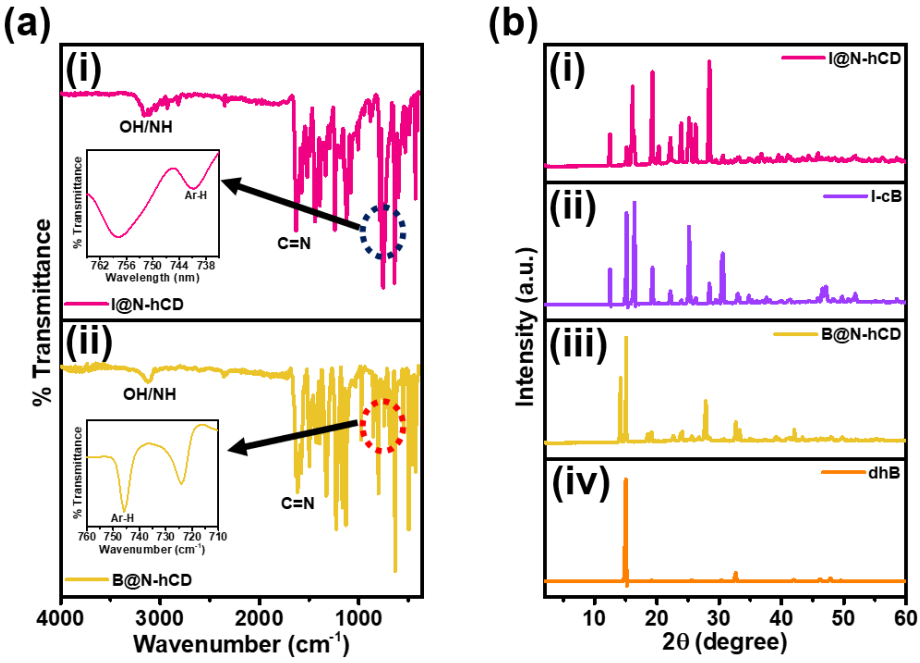

Figure 7. (a) FT-IR spectra of (i) I@N-hCDs and (ii) B@N-hCDs, (b) PXRD pattern of (i) I@N-hCDs, (ii) I-cB, (iii) B@N-hCDs, and (iv) dhB.

Further, the AIE trait of I@N-hCDs and B@N-hCDs was checked. For this, both the powders were added in different ratios of EtOH and H_2O. Figure 8a and b illustrate that the I@N-hCDs and B@N-hCDs could be evenly dispersed in ethanol but not in water and form aggregates. On increasing the water percentage, from 0 to 100, the CDs reveal two-dimensional layered structures as shown in Figures 8c and d. The SEM and confocal studies of the dispersion of I@N-hCDs and B@N-hCDs, separately in water, were also performed, and it was observed that both showed 2D rod-like assemblies, as depicted in Figures 8c-f, respectively. The TGA curves for I@N-hCDs and B@N-hCDs are given in Figures 9i and ii. The thermogram of B@N-hCDs proved that it is thermally

stable up to 120 °C; however, I@N-hCDs exhibited thermal stability up to 155 °C, demonstrating that the SSF powders can maintain exceptional thermal stability across a large temperature range.

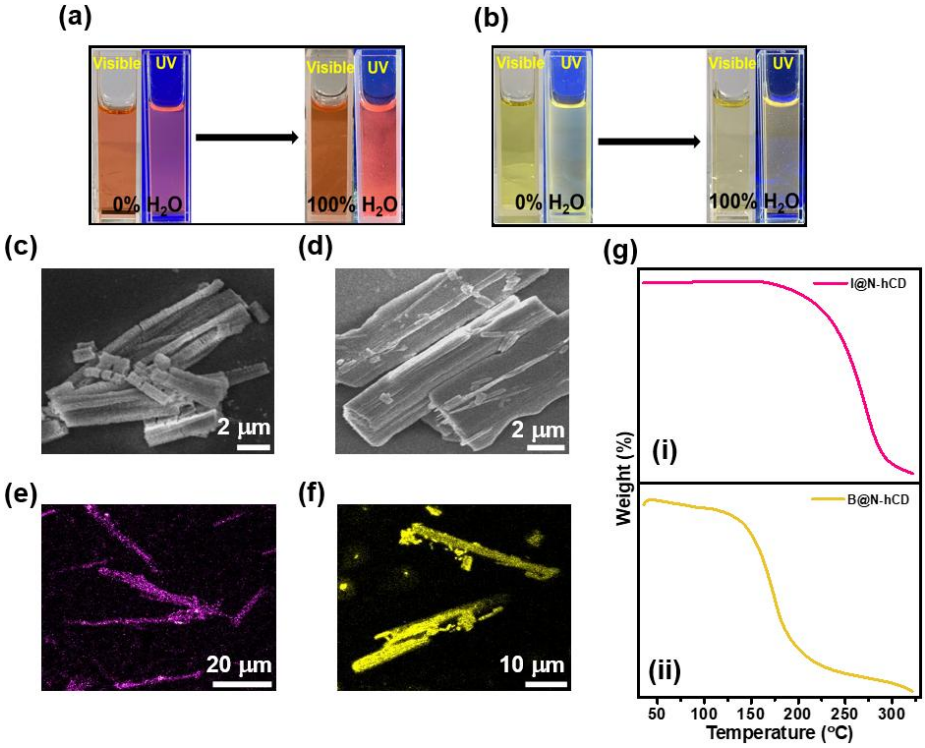

Figure 8. Photo images of (a) I@N-hCDs and (b) B@N-hCDs in EtOH (left) and H_2O (right) under visible and 365 nm irradiation. SEM images of (c) I@N-hCDs and (d) B@N-hCDs after being dispersed in water, confocal fluorescence images of (e) I@N-hCDs and (f) B@N-hCDs, (g) TGA curves of (i) I@N-hCDs and (ii) I@N-hCDs.

6.6 Application for Latent fingerprint visualization and identification

6.6.1 LFP Visualization with B@N-hCDs and I@N-hCDs

The synthesized powders B@N-hCDs and I@N-CDs, bearing excellent solid-state FL, are used to visualize the LFPs. For this purpose, the powder method is employed on distinct substrates to check the feasibility of the SSF powders for the development of FPs. The SSF powder was spread around the LFP and developed by spreading it all over the LFP with the help of a soft feather brush, giving tint to the FPs, and the excess powder was cautiously brushed off with a soft feather brush. The images obtained are observed under visible and UV light, and

captured the images for further analysis. Moreover, the FPs were developed with the help of B@N-hCDs and I@N-hCDs on various surfaces such as glass slide, aluminum foil, stainless steel bottle, cover slip, and amber colour glass bottle with the powder method mentioned above. Further, the obtained fingerprints are visualized under visible and UV light as shown in Figures 9 (B@N-hCDs) and Figure 10 (I@N-CDs). The obtained images were further analysed to know about the developed pattern, which is indicative of an ulnar loop, and also the next level characterization present on a person's finger. The results indicate that the distinction between level I, II, and III details procured from an individual's fingerprint can be distinctly displayed on given substrates.

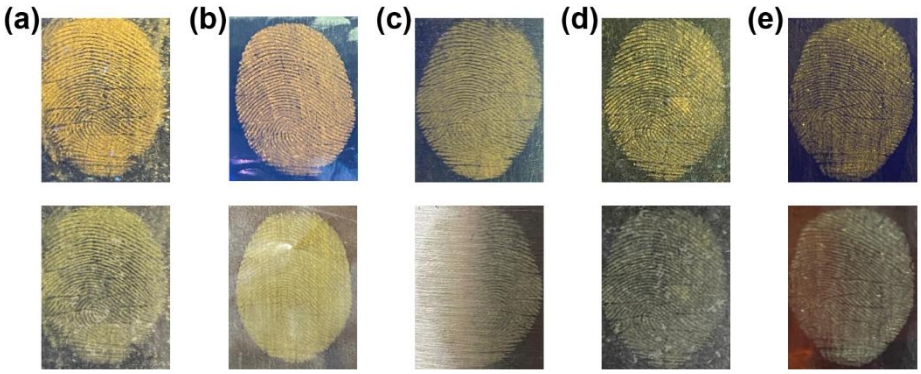

Figure 9. Developed fingerprint images of B@N-hCDs on (a) glass slide, (b) aluminum foil, (c) stainless steel bottle, (d) cover slip, and (e) glass bottle of chemical under UV irradiation (upper) and visible light (lower)

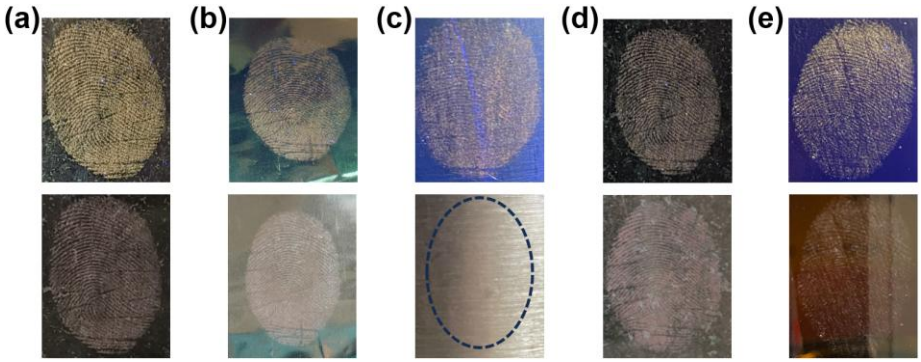

Figure 10. Developed fingerprint images of I@N-hCDs on (a) glass slide, (b) aluminum foil, (c) stainless steel bottle, (d) cover slip, and (e)

glass bottle of chemical under UV irradiation (upper) and visible light (lower)

6.6.2 Separation of Ridge features

The certainty of the extraction of the three-level properties of FPs by a powder shows the efficiency of the SSF powder. The level I traits include a loop, arch, compound, and whorl. Moreover, ridge dots, eye, islands, short ridge, core, bifurcations, lakes, folds of ridges and rift valleys of furrows, terminations, hook, and crossover double bifurcation are included in level II. Additionally, level III covers minuscule details such as the length and breadth of the ridge, scars, sweat pores, ridge end form, shape, size, sweat pores, etc.[4,41] All three pieces of information are deeply analyzed, which enables the identification of an individual.

The magnified images depicting the details of the three levels of the FP developed by B@N-hCDs on aluminum foil are shown in Figure 11. Moreover, level II details indicate that the core, island, bifurcation, hook, and termination can be viewed through the naked eye. In addition, the insights on level III (sweat pores and scar) could be seen, which is crucial for a person's identity.

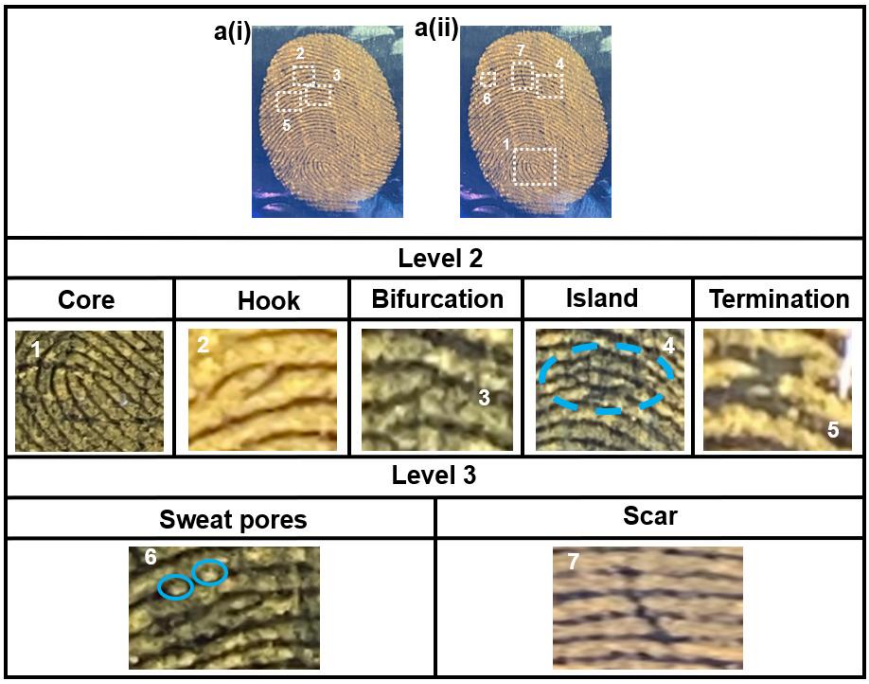

Figure 11. (ai, ii) Images of LFPs on the aluminum foil developed through powder method with B@N-hCDs under UV light. The magnified images show specific details as listed below: (1) core, (2) hook, (3) bifurcation, (4) island, (5) termination, (6) sweat pores, and (7) scar.

The magnified images depicting the details of the three levels of the FP developed by I@N-hCDs on a glass slide are shown in Figure 12. Moreover, level II details indicate island, core, crossover, and termination can be viewed through the naked eye. In addition, the insights on level III (sweat pores and scar) could be seen, which is crucial for a person's identity.

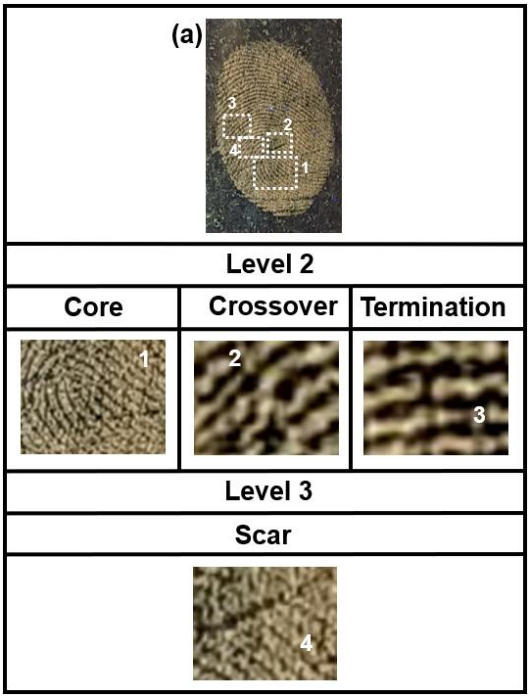

Figure 12. Images of LFPs on the glass slide developed through the powder method with I@N-hCDs under UV light. The magnified images show specific details as listed below: (1) core, (2) crossover, (3) termination, and (4) scar.

These outcomes imply that the SSF powders B@N-hCDs and I@N-hCDs with color-tunable emission are viable for at crime scenes for fingerprint development on various surfaces, showing different contrast.

Table 3 indicates the comparative reports for CDs-based composites with solid-state FL for LFP identification on various surfaces.

S. No	CDs based composites	QY (%)	λ_{em} (nm)	Substrates used	References
1.	CDs/SiO_2	37	470	Glass, aluminum foil, black plastic bags, drug packing, and leather	*Anal. Methods* **2017**, *9*, 4770-4775
2.	CDs@PGV nanocomposites	1.93	447	Painted metal, glass, plastic products, plastic label paper, and stainless steel	*Bull. Chem. Soc. Jpn.* **2017**, *90*, 1217–1223
3.	N, S-SFCDs	48.1	460-600	Printing paper, plastics, aluminum foil, glass, ceramic, and steel	*Part. Part. Syst. Charact* **2018**, *35*, 1700387–1700394
4.	O-CDs, G-CDs	28.5, 83	603, 512	Aluminum foil, glass, and plastic	*ACS Appl. Nano Mater.* **2019**, 2, 5900–5909
5.	R-CDs/ starch phosphors	21	620	Glass, paper, and plastic substrates	*ACS Appl. Mater. Interfaces* **2020**, *12*, 29549-29555
6.	RP-CDs	-	585	Compact disc upper face, compact disc glossy face, plastic bottle, aluminum foil, glass petri dish, lock, and tiffin box	*New J. Chem.* **2023**, *47*, 17110-17119
7.	R6G-CDs4/DE and RB-CDs4/DE	4.53 and 7.31	559 and 544-572	Glazed ceramic tiles, patterned plastic films, plastic packing printed with words, glass sheets, and stainless-steel sheets	*ACS Sustainable Chem. Eng.* **2022**, 10, 43, 14294–14308
8.	CDs@PVP	6.33, 16.5, and 43.6	612, 591, and 559	Glass glide, ceramic tile, painted wood, aluminum alloy plate, and banknote	*ACS Appl. Nano Mater.* **2022**, *5*, 2214−2221
9.	B@N-hCDs and I@N-hCDs	3.52 and 4.22	520 and 625	Glass slide, aluminum foil, glass chemical bottle, steel bottle, cover slip	Our work

Table 3. List of CD-based composites with SSF used for LFP visualization on various surfaces.

Chapter 7

CONCLUSIONS AND SCOPE OF WORK

In summary, novel, solid, matrix-free SSF CDs with multicolor FL were synthesized by a surface ligand modulation strategy, which exhibited excellent photoluminescence properties. In this work, the carbon dots were synthesized through a one-step hydrothermal method using potassium humate and o-phenylenediamine as carbon and nitrogen sources, respectively. To address fluorescence quenching caused by aggregation in solid-state, various surface functionalization strategies were employed, including the use of 2,4-dihydroxybenzaldehyde and Indole-3-carboxaldehyde, which overcome the aggregation-induced fluorescence quenching of CDs in a solid state, which also enabling aggregation-induced emission with improved stability in the solid state. Adjustment of ligands could tune the emission color of the CDs' SSF from yellow to pink. The developed SSF CDs have a great potential applicability for fingerprint identification. The SSF CDs can also be utilized for the development and visualization of LFP on various substrates. Therefore, this work provides a superior and universal fluorescent developer, which can also be applied to observing minute LPF details for individualization and thus showing great potential in forensic investigation. Moreover, from a future standpoint, by refining the functionalization strategy and exploring various CDs and ligands, one could synthesize a range of SSF CDs with fluorescence properties spanning from blue to red and utilize them further on various porous and nonporous surfaces.

REFERENCES

(1) Wang, R.; Huang, Z.; Ding, L.; Yang, F.; Peng, D. Carbon Dot Powders with Cross-Linking-Based Long-Wavelength Emission for Multicolor Imaging of Latent Fingerprints. *ACS Appl. Nano Mater*. **2022**, *5* (2), 2214–2221.

(2) Ruan, N.; Qiu, Q.; Wei, X.; Liu, J.; Wu, L.; Jia, N.; Huang, C.; James, T. D. De Novo Green Fluorescent Protein Chromophore-Based Probes for Capturing Latent Fingerprints Using a Portable System. *J. Am. Chem. Soc*. **2024**, *146* (3), 2072–2079.

(3) Yuan, C.; Wang, M.; Li, M.; Sun, P.; Gao, R.; Tang, J. Construction, Mechanism, and Forensic Application of Green-Light-Excited Fluorescent Carbon Dots/Diatomite Composites. *ACS Sustainable Chem. Eng*. **2022**, *10* (43), 14294–14308.

(4) Swathi, B. N.; Krushna, B. R. R.; Manjunatha, K.; Lo, W.-C.; Hsu, T.-E.; Jheng, C.-Y.; Ho, M.-K.; Chiu, H.-H.; Yu, S.-L.; Huang, Y.-L.; Sharma, S. C.; Subramanian, B.; Wu, S. Y.; Nagabhushana, H. Orange–Red Emitting Sr9Al6O18:Pr3+ Nanophosphors for Advanced Latent Fingerprints and Security Ink. *ACS Appl. Nano Mater*. **2023**, *6* (22), 21322–21339.

(5) Peng, D.; Huang, M.; Xiao, Y.; Zhang, Y.; Lei, L.; Zhu, J. Highly-Selective Recognition of Latent Fingermarks by La-Sensitized Ce Nanocomposites via Electrostatic Binding. *Chemical Communications* **2019**, *55* (71), 10579–10582.

(6) Wang, J.; Peng, R.; Luo, Y.; Wu, Q.; Cui, Q. Preparation of Fluorescent Conjugated Polymer Micelles with Multi-Color Emission for Latent Fingerprint Imaging. *Colloids and Surfaces A: Physicochemical and Engineering Aspects* **2021**, *615*, 126192.

(7) Li, M.; Tian, T.; Zeng, Y.; Zhu, S.; Lu, J.; Yang, J.; Li, C.; Yin, Y.; Li, G. Individual Cloud-Based Fingerprint Operation Platform for Latent

Fingerprint Identification Using Perovskite Nanocrystals as Eikonogen. *ACS Appl. Mater. Interfaces* **2020**, *12* (11), 13494–13502.

(8) Yang, H.; Yang, X.; Zhang, Q.; Lu, D.; Wang, W.; Zhang, H.; Yu, Y.; Liu, X.; Zhang, A.; Liu, Q.; Jiang, G. Precisely Identifying the Sources of Magnetic Particles by Hierarchical Classification-Aided Isotopic Fingerprinting. *Environ. Sci. Technol*. **2024**, *58* (22), 9770–9781.

(9) Pavitra, E.; Raju, G. S. R.; Park, J. Y.; Hussain, S. K.; Chodankar, N. R.; Rao, G. M.; Han, Y.-K.; Huh, Y. S. An Efficient Far-Red Emitting Ba2LaNbO6:Mn4+ Nanophosphor for Forensic Latent Fingerprint Detection and Horticulture Lighting Applications. *Ceramics International* **2020**, *46* (7), 9802–9809.

(10) Li, Y.; Xu, L.; Su, B. Aggregation Induced Emission for the Recognition of Latent Fingerprints. *Chem. Commun*. **2012**, *48* (34), 4109–4111.

(11) Ai, L.; Song, Z.; Nie, M.; Yu, J.; Liu, F.; Song, H.; Zhang, B.; Waterhouse, G. I. N.; Lu, S. Solid-State Fluorescence from Carbon Dots Widely Tunable from Blue to Deep Red through Surface Ligand Modulation. *Angewandte Chemie International Edition* **2023**, *62* (12), e202217822.

(12) Wang, H.; Liu, G. Advances in Luminescent Materials with Aggregation-Induced Emission (AIE) Properties for Biomedical Applications. *J. Mater. Chem. B* **2018**, *6* (24), 4029–4042.

(13) Singla, N.; Kaur, M.; Sofat, S. Automated Latent Fingerprint Identification System: A Review. *Forensic Sci Int* **2020**, *309*, 110187.

(14) Stojanović, B.; Marques, O.; Nešković, A. Latent Overlapped Fingerprint Separation: *A Review. Multimed Tools Appl* **2017**, *76* (15), 16263–16290.

(15) Huynh, C.; Halámek, J. Trends in Fingerprint Analysis. *TrAC Trends in Analytical Chemistry* **2016**, *82*, 328–336.

(16) Sodhi, G. S.; Kaur, J. Physical Developer Method for Detection of Latent Fingerprints: A Review. *Egyptian Journal of Forensic Sciences* **2016**, *6* (2), 44–47.

(17) Sekar, A.; Vadivel, R.; Munuswamy, R. G.; Yadav, R. Fluorescence Spotting of Latent Sweat Fingerprints with Zinc Oxide Carbon Dots Embedded in a Silica Gel Nanopowder: A Green Approach. *New J. Chem*. **2021**, *45* (37), 17447–17460.

(18) Xu, K.; Chen, G.; Zhao, M.; He, W.; Hu, Q.; Pu, Y. Transparent, Self-Recoverable, Highly Tough, Puncture and Tear Resistant Polyurethane Supramolecular Elastomer with Fast Self-Healing Capacity via "Hard–Soft" Hard Domain Design. *RSC Adv*. **2022**, *12* (5), 2712–2720.

(19) Wei, T.; Han, J.; Wang, L.; Tao, J.; Zhang, H.; Xu, D.; Su, S.; Fan, C.; Bi, W.; Sun, C. Magnetic Perovskite Nanoparticles for Latent Fingerprint Detection. *Nanoscale* **2021**, *13* (27), 12038–12044.

(20) Oden, S.; Von Hofsten, B. Detection of Fingerprints by the Ninhydrin Reaction. *Nature* **1954**, *173* (4401), 449–450.

(21) Jasuja, O. P.; Kaur, A.; Kumar, P. Fixing Latent Fingermarks Developed by Iodine Fuming: A New Method. *Forensic Science International* **2012**, *223* (1), 47–52.

(22) Vadivel, R.; Nirmala, M. Visualization of Latent Fingerprints Using Neutral Alumina as an Inexpensive Fingerprint Developing Powder. *Research Gate* **2020**, 5-10.

(23) Shabashini, A.; Panja, S. K.; Nandi, G. C. Applications of Carbon Dots (CDs) in Latent Fingerprints Imaging. *Chem. Asian J*. **2021**, *16* (9), 1057-1072.

(24) Mate, N.; Khandelwal, D.; Nabeela, K.; Mobin, S. M. Portable and Non-Invasive Fluorescent Thin Films from Photocatalytically Active Carbon Dots for Selective and Trace-Level Detection of Picric Acid. *J. Mater. Chem. C* **2023**, *11* (46), 16201–16213.

(25) Dong, X.-Y.; Niu, X.-Q.; Zhang, Z.-Y.; Wei, J.-S.; Xiong, H.-M. Red Fluorescent Carbon Dot Powder for Accurate Latent Fingerprint Identification Using an Artificial Intelligence Program. *ACS Appl. Mater. Interfaces* **2020**, *12* (26), 29549–29555.

(26) Di, L.; Xing, Y.; Yang, Z.; Qiao, C.; Xia, Z. Photostable Aggregation-Induced Emission of Iridium (III) Complex Realizing Robust and High-Resolution Imaging of Latent Fingerprints. Sensors and Actuators B: Chemical 2023, 375, 132898.

(27) Bleay, S. M.; Bailey, M. J.; Croxton, R. S.; Francese, S. The Forensic Exploitation of Fingermark Chemistry: A Review. *WIREs Forensic Science* **2021**, *3* (4), e1403.

(28) Wan, J.; Chen, L.; Li, W.; Cui, S.; Yuan, B. Preparation of Novel Magnetic Nanomaterials Based on "Facile Coprecipitation" for Developing Latent Fingerprints (LFP) in Crime Scenes. *ACS Omega* **2022**, *7* (2), 1712–1721.

(29) Tang, X.-D.; Yu, H.-M.; Nguyen, W.; Amador, E.; Cui, S.-P.; Ma, K.; Chen, M.-L.; Wang, S.-Y.; Hu, Z.-Z.; Chen, W. New Observations on Concentration-Regulated Carbon Dots. *Advanced Photonics Research* **2023**, *4* (3), 2200314.

(30) Ai, L.; Song, Z.; Nie, M.; Yu, J.; Liu, F.; Song, H.; Zhang, B.; Waterhouse, G. I. N.; Lu, S. Solid-State Fluorescence from Carbon Dots Widely Tunable from Blue to Deep Red through Surface Ligand Modulation. *Angewandte Chemie International Edition* **2023**, *62* (12), e202217822.

(31) Sun, M.; Qu, S.; Hao, Z.; Ji, W.; Jing, P.; Zhang, H.; Zhang, L.; Zhao, J.; Shen, D. Towards Efficient Solid-State Photoluminescence Based on Carbon-Nanodots and Starch Composites. *Nanoscale* **2014**, *6* (21), 13076–13081.

(32) Wang, J.; Zheng, J.; Yang, Y.; Liu, X.; Qiu, J.; Tian, Y. Tunable Full-Color Solid-State Fluorescent Carbon Dots for Light Emitting Diodes. *Carbon* **2022**, *190*, 22–31.

(33) Park, J. H.; Cho, D. H.; Moon, Y.; Shin, H. C.; Ahn, S. J.; Kwak, S. K.; Shin, H. J.; Lee, C.; Ahn, J. R. Designed three-dimensional freestanding single-crystal carbon architectures. *ACS nano* **2014**, *8* (11), 11657–11665.

(34) Lou, X. Y.; Yang, Y. W. Manipulating Aggregation-Induced Emission with Supramolecular Macrocycles. *Adv. Opt. Mater*. **2018**, *6*, 1800668.

(35) Nguyen, K.G., Baragau, IA., Gromicova, R. *et al.* Investigating the effect of N-doping on carbon quantum dots structure, optical properties and metal ion screening. *Sci Rep* **2022,** *12*, 13806.

(36) Mohandoss, S.; Palanisamy, S.; Priya, V. V.; Mohan, S. K.; Shim, J.-J.; Yelithao, K.; You, S.; Lee, Y. R. Excitation-Dependent Multiple Luminescence Emission of Nitrogen and Sulfur Co-Doped Carbon Dots for Cysteine Sensing, Bioimaging, and Photoluminescent Ink Applications. *Microchemical Journal* **2021**, *167*, 106280.

(37) Mate, N.; Khandelwal, D.; Nabeela, K.; Mobin, S. M. Portable and Non-Invasive Fluorescent Thin Films from Photocatalytically Active Carbon Dots for Selective and Trace-Level Detection of Picric Acid. *J. Mater. Chem. C* **2023**, *11* (46), 16201–16213.

(38) Wang, H.-J.; Yu, T.-T.; Chen, H.-L.; Nan, W.-B.; Xie, L.-Q.; Zhang, Q.-Q. A Self-Quenching-Resistant Carbon Dots Powder with Tunable Solid-State Fluorescence and Their Applications in Light-Emitting Diodes and Fingerprints Detection. *Dyes and Pigments* **2018**, *159*, 245–251.

(39) Gao, J.; Zhu, M.; Huang, H.; Liu, Y.; Kang, Z. Advances, Challenges and Promises of Carbon Dots. *Inorg. Chem. Front*. **2017**, *4* (12), 1963–1986.

(40) Chen, B. B.; Liu, M. L.; Li, C. M.; Huang, C. Z. Fluorescent Carbon Dots Functionalization. *Advances in Colloid and Interface Science* **2019**, *270*, 165–190.

(41) Wang, C.; Zhou, J.; Lulu, L.; Song, Q. Rapid Visualization of Latent Fingerprints with Color-Tunable Solid Fluorescent Carbon Dots. *Particle & Particle Systems Characterization* **2018**, *35* (3), 1700387.